Shock-wave interaction with reduced-scale simplified torso surrogates

Johanna Boutillier, Sébastien De Mezzo, Caroline Deck, Loïc Ehrhardt,
Pascal Magnan, Pierre Naz, Rémy Willinger

Abstract The main objectives of this study are to understand the complex shockwave-structure interaction, in addition to the influence of the side-on pressure profile generated by the detonation of an explosive charge on simplified torso surrogates' responses. To achieve those objectives, rigid and deformable rectangular parallelepipeds (RPP) and cylinders were exposed to a spherical explosive charge of C-4 of 0.3 kg at three different heights of burst. With pressure gauges positioned flush with the structures surfaces at different locations and an accelerometer to measure the kinematic parameters on the deformable torso surrogates, four hundred fifteen reproducible measurements were obtained. The cylinder model showed reduced impulses, accelerations, velocities and displacements compared to the RPP which offers more resistance to the blast. From the deformable surrogates, it was shown that the peak of acceleration is influenced by the pressure-time history despite similar maximum impulses, which is not the case for the velocity and the displacement. It is inferred from this that the peak of acceleration, sometimes used to evaluate protective systems, seems not so good a metric that expected to quantify the changes in lung injury by wearing protective clothing. However, the maximum of velocity and displacement seems to be good candidate parameters for thoracic injury criteria definition.

Keywords Shock-wave interaction, torso surrogates, experimentation, pressure-profile influence

I. INTRODUCTION

The detonation of an explosive charge generates the propagation of a shock-wave, principally affecting gas-containing organs, such as lungs, middle ear and gastrointestinal tract [1-2]. In a free-field environment, the pressure-time history resulting from a detonation has a well-known shape, called the Friedlander profile [1]. The use of Improvised Explosive Devices (IED) became the an important cause of injuries on the battlefield, which represent up to 60 % of the number of death among the US forces during Operation Enduring Freedom in Afghanistan [3-4]. In this soldier and law enforcement safety context, it is important to evaluate the load of Friedlander wave and of more complex ones, on a torso surrogate. It is a key step to understand the influence of textile layers and protective systems on thorax injuries degree. Indeed, the unprotected torso surrogate response to such threats much first be known to then evaluate the influence of protective clothing on the surrogate's response.

Three main test methods are currently used to assess the loading that would have faced a human thorax [5-8]. Simplified rigid and deformable thorax models have been developed to record the pressure at different locations, as well as the motion of those surrogates for blast studies. The Blast Test Device (BTD) is a hollow rigid cylinder of 76 cm height with a 30 cm diameter, representative of a human thorax. It is instrumented with pressure gauges every 90 degree interval at mid-height. In Johnson experiments [5], this surrogate was placed in similar scenarios as sheep in a confined space. The obtained pressure profiles and lung injury levels on sheep were then used as calibration data for the Axelsson and Stuhmiller injury prediction models [9-10]. The BTD is also used in numerical simulations in order to evaluate the influence of its position in the environment on the measured pressure [11-12]. Those studies allowed the improvement of injury criteria, such as the Bowen and Bass curves [13-14]. Another simplified version of a human torso is the Canadian "U"-shape deformable membrane, made of elastomer of polyurethane (PMC 870). With a length of 55 cm, a width of 38.5 cm and a thickness of 20 cm, this membrane is validated for non-lethal projectile impact. This simplified model was also used in blast study to evaluate the loading, with and without protective equipment [7][15]. More recently, Defense Research and Development Canada (DRDC) developed an anthropomorphic mannequin in elastomer of

J. Boutillier (e-mail: jboutillier1@gmail.com; tel: 00 333 68 85 29 43) is a Ph.D. student, C. Deck is a Ph.D. researcher and R. Willinger is Professor in Biomechanics at ICube Laboratory, University of Strasbourg. S. De Mezzo is an engineer, L. Ehrhardt is an assistant researcher, P. Magnan is a researcher and P. Naz is the head of the group "Acoustics and Protection of the Soldier" group at the French-German Research Institute of Saint Louis (ISL).

polyurethane (PMC 870) (50th percentile), called Mannequin for the Assessment of Blast Incapacitation and Lethality (MABIL). It was not built to mimic the response of biological surrogates, but to qualitatively assess the efficiency of protective systems [8][16]. Its shape is based on the 1988 US Army ANSUR anthropometric database, and the membrane thickness at the front and side is 20 mm, similar to the "U"-shape membrane. With the use of that anthropomorphic dummy, protective system evaluation was performed [8]. The authors demonstrated that thoracic wall velocity, the parameter used in the Axelsson prediction model, is not a good metric for that specific aim. Nevertheless, thoracic wall's peak of acceleration could be a good candidate parameter to differentiate protective vests, but no blast injury criteria were developed in order to use that parameter. However, it seems important to quantitatively evaluate the changes in injury by wearing a protective cloth, although none of the existing injury criteria seems adapted for this specific topic [17].

Friedlander waveform is commonly used for those blast interaction studies, but a soldier does not only face those idealised shocks. Reflections of the wave on the ground or in any obstacles are factors that complicate the pressure-time histories. The influence of a complexification on the pressure profiles recorded on the surrogates and on its motion is still unknown and should be investigated.

This study focuses on blast interaction with rigid and deformable reduced-scale simplified torso surrogates inspired from the simple torso versions described previously. A rectangular parallelepiped (RPP) and a cylinder will then be studied. Because of a lack of free-field experimental ground availability, reduced-scale experiments were preferred to full-scaled experiments. To reproduce scenarios that can be seen on the battlefield, three different scenarios will be investigated: a charge close to the ground; a charge at mid-sternum human height; and finally, an intermediate configuration will be performed. A previous study was performed to get a side-on pressure cartography with those heights of burst (HoB) using five different masses of C-4 [18]. As the charge limit here is 0.3 kg of C-4, a scaled factor of 2/3 was chosen to reproduce a scenario realised in that cartography of pressure, where the triple-point paths were obtained. Using those triple-point paths, the location of the surrogates was determined. Then, going from a HoB close to the ground from the highest one tested will change the pressure profile from a Friedlander waveform to an incident wave followed by its reflection from the ground. The aim is to evaluate the changes in pressure and kinematic parameters (acceleration, velocity and displacement) for the different tested shapes when the side-on pressure profile become more complex. The obtained pressure data give indication of the pressure waveform around structure closer in shape to a simplified thorax, and will then be used to evaluate numerically blast structures interaction with different numerical codes (LS-DYNA and an home-made code, called BSM [19]).

II. METHODS

This section describes the structures developed in the present study and exposed to several shock-waves, as well as their instrumentation. In addition, it also describes the setup and the performed scenarios.

The reduced-scale simplified torso surrogates

With the aim of understanding the influence of the target's shape on the loading and its response, four different structures whose shape becomes closer to a simplified thorax geometry were exposed to shock-waves. The dimensions of the structure in that study are related to the scaled height of the "U"-shape membrane and to the scaled diameter of the BTD. Two types of shape structure were used: a hollow rectangular parallelepiped (RPP) with 20 cm width and length; and a hollow cylinder of 20 cm diameter. The height of both models is 37.5 cm. For each shape of structures, Dural® material and steel are used for the rigid versions and elastomer of polyurethane material (PMC 770) [20] is used for the deformable models (Fig. 1). The deformable membranes are 13 mm thick, in accordance with the scaled thickness of the "U"-shape membrane and MABIL.

The RPP is made of a metallic frame on which four 7 mm thick Dural® plates are screwed. Only the exposed face will be changed by a 13 mm thick plate of PMC 770 for the deformable surrogates. Not to change the dimensions of the RPP between the rigid and deformable models, the exposed face for the rigid RPP is also 13 mm thick. The complete structure (mass 10.5 kg) is then screwed on a steel cylindrical support with a height of 70 cm and a diameter of 7 cm. For the deformable structure (mass 6.5 kg), only the front face was replaced with a 13 mm thick deformable plate, sandwiched by a 2 mm thick metallic frame in order to maintain it, as illustrate the Figure 2.

The rigid cylinder (mass 28.8 kg) was manufactured from a solid steel cylinder. The final thickness was 13 mm. Cylindrical plates and a thread rod were used to fix the structure with the support and to close it. Similarly to the RPP, the complete structure is screwed on the same cylindrical support. The difference is in the extremity supporting the target. Indeed, the base is now circular, with the same diameter as the cylinder. For the deformable cylinder (mass 10.0 kg), only the cylindrical part was replaced with its elastomer version. The two rigid thrust washers and the metallic rod passing through them help to maintain the global shape at rest, as well as during the interaction with the shock-wave.

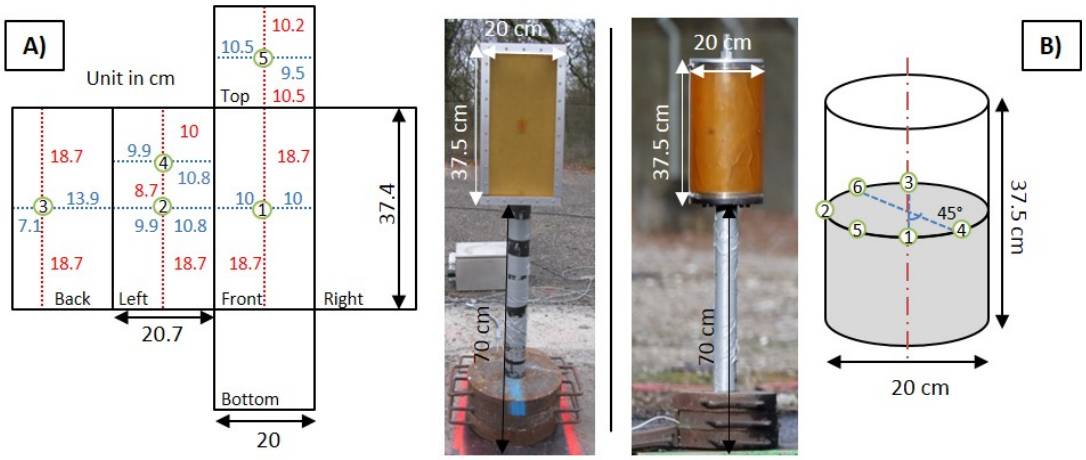

Fig. 1. Illustration of the (A) deformable RPP and (B) the cylinder, with all dimensions. The schemes show the location of the pressure probes for the rigid and deformable surrogates. Sensor (1) correspond to a piezo-resistive pressure transducer (Kulite XT190M) + one piezoelectric charge accelerometer (B&K 8309, only for deformable targets). Sensors 2 to 6 are piezo-resistive pressure transducers (Kulite XT190M).

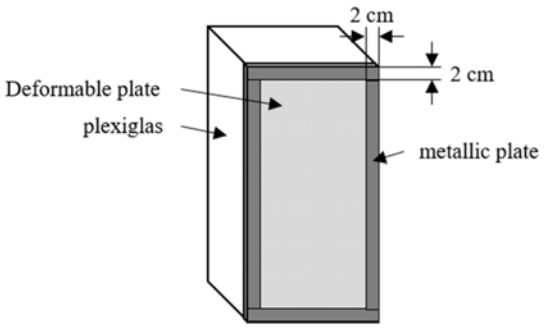

Fig. 2. Illustration of the fixation of the deformable plate on the RPP model.

Instrumentation used

For the rigid surrogates, five (for the RPP) and six (for the cylinder) piezo-resistive sensors (Kulite XT 190M, 35 bar) were disposed all around the surrogates to record the pressure-time histories. Eight millimeter holes were made in the desired gauges location, as illustrated in Fig 1, to receive the sensors, beforehand put in an adapted support as its length was higher than the plate thickness. The sensitive part of the sensor is covered with a thermal protection and is flush with the external surfaces.

For the deformable structures, the Kulite XT 190M pressure probes are screwed in the membrane and secured with elastomer of polyurethane, to ensure they do not come out of the holes during the exposure. The piezoelectric charge accelerometers B&K 8309 used were fixed with the elastomer of polyurethane in the centre of back of the loaded part. His ranges cover 2E-3 G to 100,000 G.

The instrumentation cables run inside the surrogates through a small hole in the supporting steel plate.
In addition to the piezo-resistive pressure sensors and piezoelectric charge accelerometer, two Free-Field Blast ICP pressure probes type 137B22 from PCB Piezotronics were used to measure the side-on pressure at the same distance from the charge as the structures.

The acquisition was made by a high-speed range data acquisition system (MF instruments), with a sampling rate of 1 MHz. The data were then filtered with a 6th order Bessel at 100 kHz for the pressure-time histories, and at 60 kHz for the acceleration pulses because some resonances were present in the acceleration measured on the RPP just after the interaction of the wave.
High-speed cameras were installed in the experimental field:

- one Phantom V1610 (black & white) (40,000 fps) is used to visualise the shock-wave propagation around the structures, made visible by the gradient-induced distortion of the background;
- two Photron RS (colour) are used (5,000 fps). One is a view of the whole scene to check the homogeneity and the sphericity of the fireball. The second is used to visualise the interaction of the shock-wave with the deformable target. It will be used in post-treatment to track the displacement of the membranes.

From those instrumentation, several parameter will be extracted. The velocity of the membranes will be obtained by time integration of the acceleration, and the displacement will be obtained from video tracking. In addition to those kinematic parameters, the Viscous Criterion is calculated for each scenario. This injury prediction criterion coming from the automotive field, developed by Lau *et al.* [21] is defined as the maximum of the product of the thorax deformation speed and the thorax deformation. The maximum of this curve (VCmax) is related to a level of injury (the AIS scoring system), a VCmax of 1 m/s will induce a 25% risk of AIS3+.

As meteorological conditions affect the blast propagation, a weather station VAISALA WXT520 was used during the experiments. It recorded the ambient pressure, temperature, wind direction and speed, humidity and rainfall.

Experimental Testing

The scenario considered in our study is the detonation of a spherical charge over a flat solid ground. This configuration generates complex behavior, depending on the mass and height of the charge, such as reflection wave or Mach reflection. The area of interest of the surrogate is at 2 m from the centre of detonation.

In order to cover a range of physical phenomena as wide as possible, different initial heights of burst (HoB) were chosen. The explosive material used is composition-4 (C-4). Its mass is 0.3 kg, and the HoB, defined here as the distance between the bottom of the charge and the ground, had three different values. HoB of 22 cm, 44 cm and 88 cm were chosen so that the structure will be impacted by waves of different pressure profiles (Fig. 3).

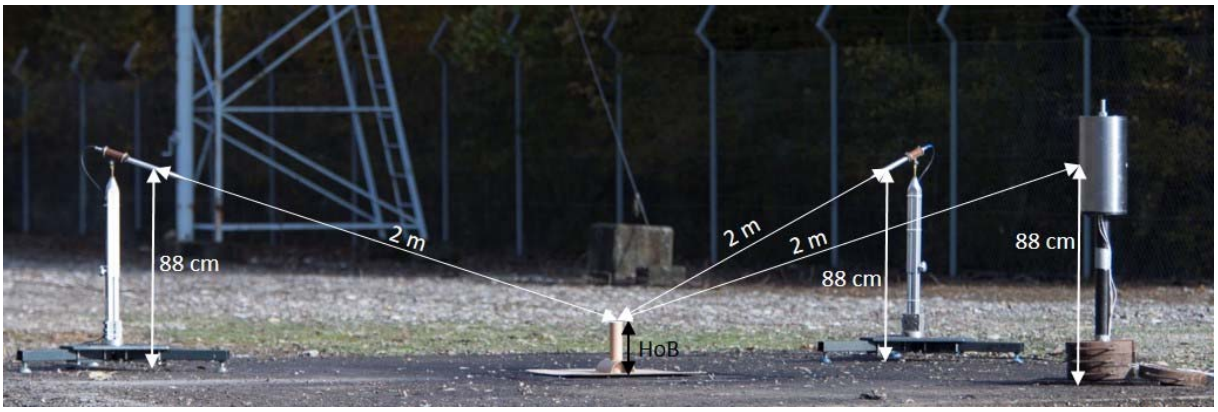

Fig. 3. Experimental setup, illustrated here with the rigid cylinder structures. The cardboard tube at the centre of the image is used to get the desired HoB.

As summarised in Table I, a total of 51 experiments were performed for the rigid surrogates, against 34 for the deformable ones, where both structures were exposed simultaneously. The number of repetitions for each scenario was at least eight. When some problem occurred during the test, such as fireball projection, an additional repetition was carried out.

TABLE I
SUMMARY OF THE EXPERIMENTAL TESTS

Scenarios	Charge radius (mm)	Number of repetitions per scenario		
		Rigid structures tests		Deformable structures tests
		RPP	Cylinder	RPP & Cylinder
0.3 kg at 22 cm	36	8	8	10
0.3 kg at 44 cm	36	9	8	11
0.3 kg at 88 cm	36	10	8	13

III. RESULTS

Three different types of loading were generated, corresponding to the three HoB used (Fig. 4). The loading from a HoB of 88 cm is the succession of a first incident wave of 91.7 ± 4.4 kPa peak pressure, followed by its reflection from the ground (74.4 ± 8.7 kPa). The smallest HoB (22 cm) corresponds to the scenario in the Mach regime. The structure will then face a unique strong overpressure (126.4 ± 5.6 kPa). The HoB of 44 cm is close to the highest one, with first incident peak of 87.5 ± 5.5 kPa, but the reflected wave of 107.0 ± 14.3 kPa peak pressure is closer to the incident one. In that configuration, the structure is in the triple-point trajectory, means that the top of the target will face two shocks (incident + reflected), while the bottom will be on the Mach stem (one strong – the strongest one).

The obtained data are reproducible, with standard deviations below 10% on the following characteristics: incident and reflected overpressures; maximum of impulse; and positive phase durations of the pressure and impulse.

Going from a HoB of 88 cm to 22 cm leads to a 38% increase in the incident overpressure, and a 14% decrease in the maximum impulse.

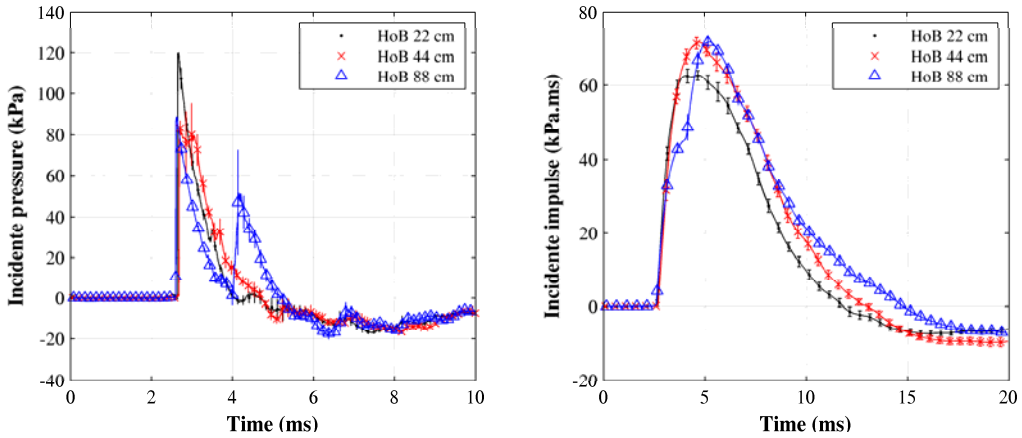

Fig. 4. Side-on pressure profiles *(left)* and impulses *(right)* for the three different heights of burst. These profiles are the mean recorded values with the standard deviation.

Influence of the shape on the pressure recorded on the rigid surrogates

Influence of the shape

Only the study on the rigid structures is used in that sub-section. Reproducible measurements were obtained, with standard deviation below 10% for the different parameters recorded, such as overpressures, positives phases durations, and maximum of impulse.

The figure 5 illustrates the pressure-time histories on the loaded and the rear (sensor not centred) faces for the HoB tested for both rigid structures (RPP and cylinder). The pressure-time histories are different according to the HoB of the explosive charge and the shape of the exposed structure. For example, the loaded surface of the RPP received two shocks of overpressures 219 ± 14 kPa and 165 ± 8 kPa respectively for a HoB of 88 cm, whereas for a HoB of 22 cm, only one highest shock (325 ± 8 kPa) is seen. However, looking at the total impulse received,

it is not significantly different for the three HoB in both models. Nevertheless, going from a HoB of 88 cm to 22 cm induce a decrease in impulse of around 20% and 15%, respectively for the RPP and the cylinder, for all the others sensors around the surrogate.

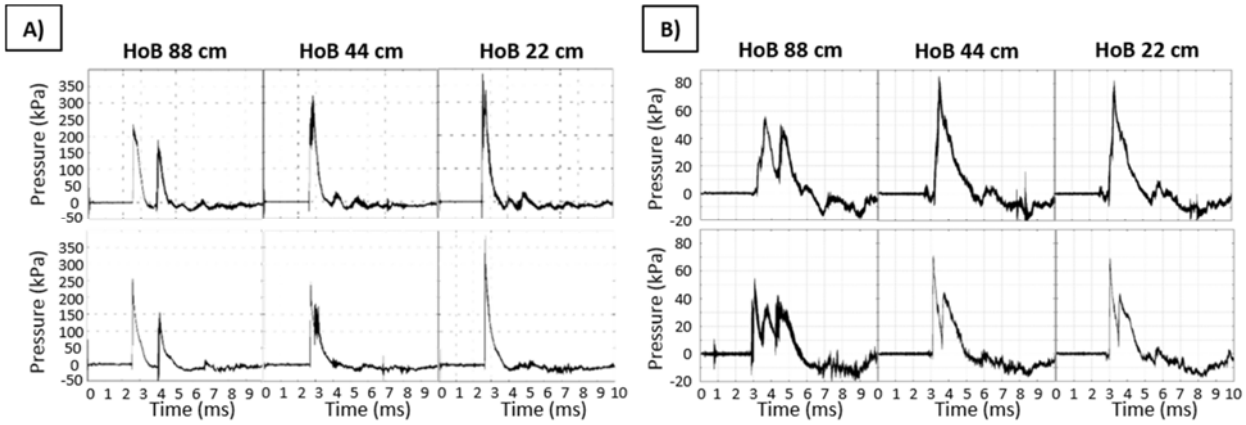

Fig. 5. (A) Pressure profiles from sensor 1 for the RPP (*top*), and for the cylinder (*bottom*). (B) Pressure profiles from sensor 3 for the RPP (*top*), and from sensor 5 for the cylinder (*bottom*).

As expected, the RPP offers more surface to the blast than the cylinder, which explains the higher impulses on its faces. Indeed, measurements on the cylinder from the three scenarios show a decrease in impulse of 18.5% on the loaded face, and up to 39.6% for the lateral face compared to the measurement on the RPP.

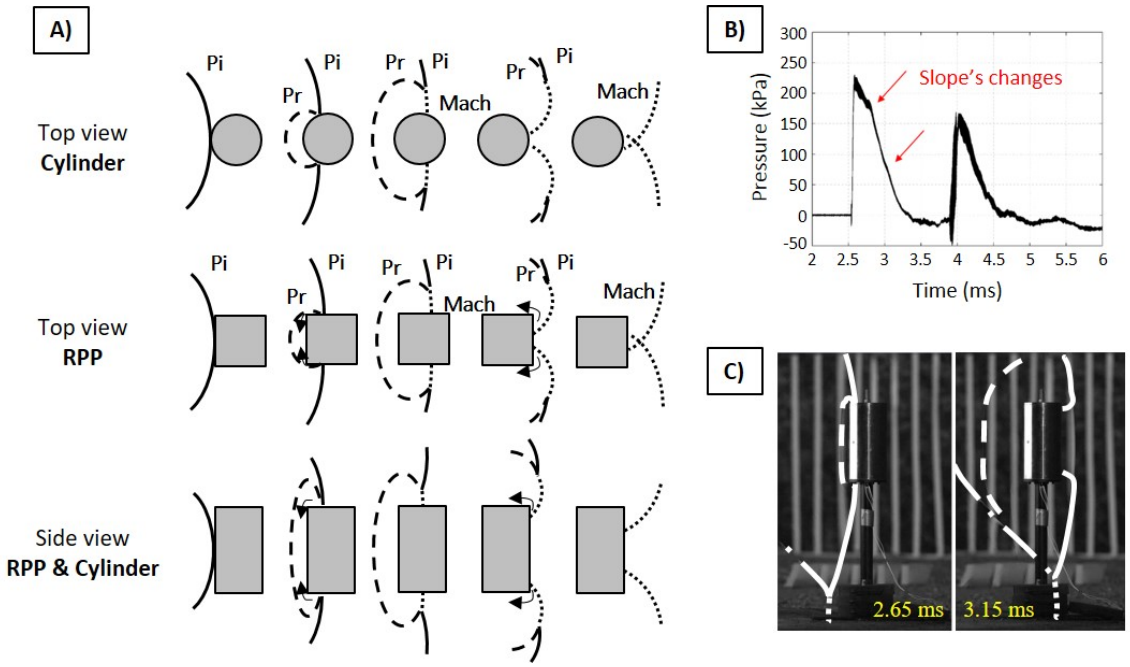

Fig. 6. (A) Bypassing of the shock-wave around the RPP and the cylinder. The arrows represent the direction of the rarefaction wave created. The formation of the Mach stem depends on the structure shape and dimension. Pi = incident pressure wave; Pr = Reflected pressure wave generated by the interaction of Pi with the structure. Each column represents the propagation at a time t. (B) Mean pressure profile of the RPP's front face, with the standard deviation. The arrows indicate the moment at which the rarefaction waves arrived, causing a decrease in the overpressure. (C) Visualisation of the shock fronts during the exposition of the cylinder to 0.3 kg at a HoB of 88 cm. This is made possible with the high cadency records from the camera (40,000 fps) and with the use of white lines in the background.

Several contributions are observed in the pressure-time histories, which can be identified, at least partially, with the use of the record from the high-speed camera at 40,000 frames per second (Fig. 6C). Those videos allow the capture of the bypassing of the wave around the structures (Fig. 6A). The diffraction phenomena can be observed, during which a rarefaction wave and a diffracted front are created. Those waves are created at the edges of the target. Indeed, the pressure difference between, for example, the loaded face by the reflected pressure (Pr) and the weak pressure at the edge (Pi) leads to the formation of those waves. In that case, the rarefaction wave is propagated through the loaded face. When the positive phase duration of the incident wave is long enough, this rarefaction wave phenomena, also called “clearing effect”, disturbs the loading in the face. This causes a decrease of the overpressure and of the positive phase duration and consequently, of the received impulse (Fig. 6B).

Pressure differences about rigid and deformable surrogates

To evaluate the influence of the material of the surrogates on the pressure level, impulse-time histories obtained on the elastomer membranes are compared with that obtained in the rigid version. For the RPPs, only the measurements from the loaded face are comparable. For the cylinder, the comparison can be performed on sensor 1, 3 and 5. Figure 7 illustrates the pressure and impulse-time histories from the RPP and the impulse-time histories from cylinder front sensor. Decreases in impulses are noticed when considering deformable structures. This decrease is greater for the RPP, which offers highest resistance to the blast, than for the cylinder.

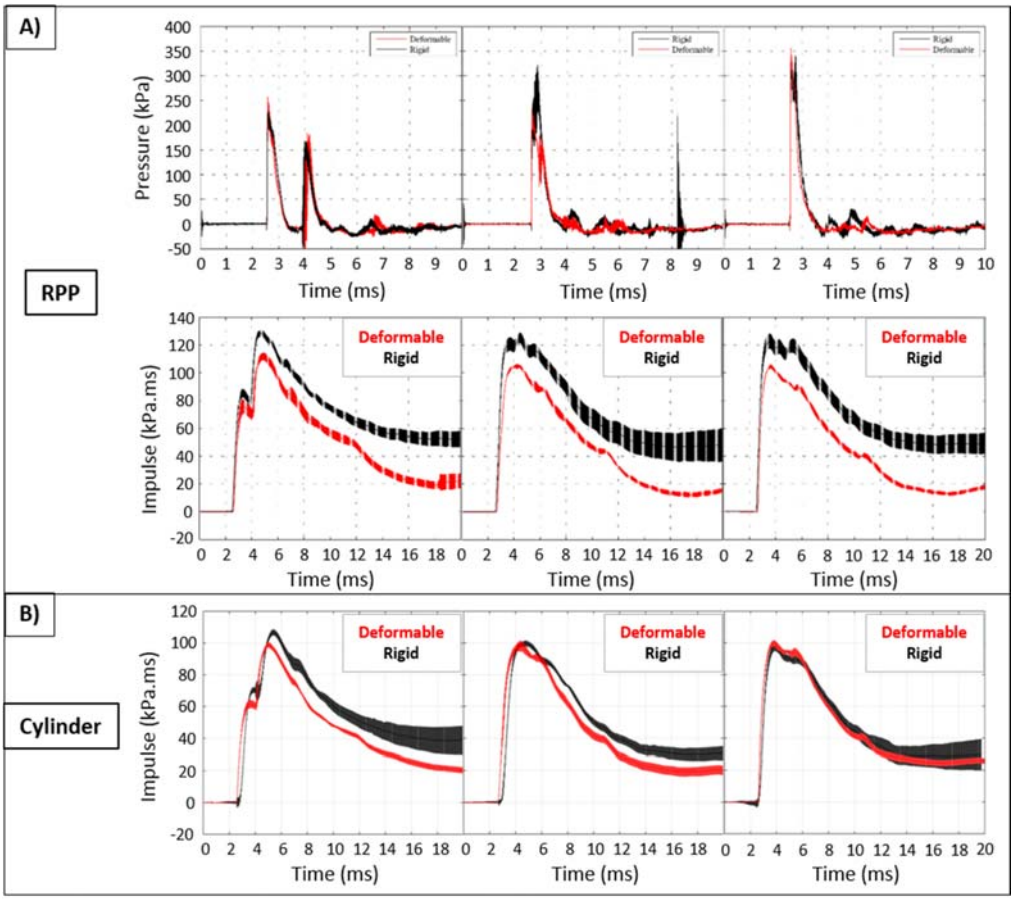

Fig. 7. (A) Pressure and Impulse received in the loaded face of the RPP; (B) Impulse received in the loaded face of the cylinder. The plotted profiles are the mean values with the standard deviations.

As illustrate the figure 7A, in each RPP case the measured overpressures were around 10% higher in the deformable case, going from 218 kPa to 239 kPa, with similar positive phase duration of 0.77 ms. However, a 15% decrease is observed in the maximum impulses. Those differences are lower with regard to the cylinder as shown the Fig. 7, with decrease of 7.8%, 1.2% and 0.8% for the HoB 88 cm, 44 cm and 22 cm respectively.

Influence of the shape and the HoB on the kinematic parameters recorded on the deformable surrogates

Influence of the HoB

Increasing the HoB of a spherical charge leads to a complexification of the side-on pressure profile. In that sub-section, the interaction of three profiles that gain in complexity with the deformable surrogates are exploited: the Friedlander waveform for the 22 cm HoB configuration; the profile in the simple reflection regime; and finally the one from the intermediate regime (HoB 44 cm).

Despite the different types of loading and with at least eight repetitions per scenario, there is no significant differences for the three HoB for both models, considering the total impulse received (108.8 ± 4.5 kPa.ms for the RPP, and 97.9 ± 4.8 kPa.ms for the cylinder). The standard deviation is around 4% in those cases. Only the shape of the profile and the time to reach that maximum is different, the latter being higher in the simple reflection regime scenario (HoB 88 cm). The maximum impulses being similar, the response in terms of acceleration, velocity and displacement can be studied for those HoB configurations.

Figure 8 shows the changes in the measured kinematic parameters and the VCmax for both structures, and for the three HoB. A decrease of 20-25% occurs in the maximum of acceleration (Γmax) when increasing the HoB from 22 cm to 88 cm. As those maxima are reached around 0.2 ms after the arrival of the side-on shock, and as the reflected wave from the ground has not yet reached the structure yet for the HoB 44 and 88 cm, this decrease was predictable. Indeed, only the first overpressure impinges the target at that time, this one being higher in the Mach stem regime (HoB 22 cm). The reflected impulse is 1.5-2 times higher in the 22 cm HoB scenario when Γmax is attained. For the VCmax, facing on strong shock or two well separated ones does not influence the injury outcomes for both torso surrogates. However, impinging the surrogates with two closed shocks is more injurious (VCmax equal to 0.65 and 0.16 at HoB 44cm for RPP and Cylinder respectively).

Nevertheless, no tendencies are found for Vmax, and Dmax. Indeed, going from 22 cm to 88 cm HoB leads to a decrease of around 20% for all cylinder's kinematic parameters. This observation is different for the RPP, with a 25% decrease in Γmax, and 9% and 7% increase in Vmax and Dmax respectively (Fig. 8).

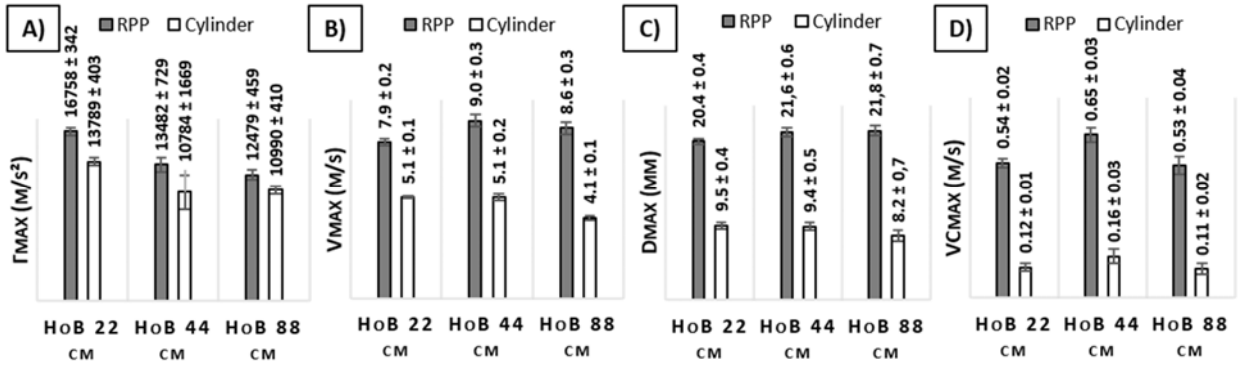

Fig. 8. Response of the RPP and the cylinder surrogates in terms of: (A) maximum of acceleration; (B) maximum of Velocity; (C) maximum of displacement; and (D) VCmax for the three HoB studied.

Influence of the shape

The kinematic parameters measured on the two simplified torso surrogates and the VCmax are plotted against the maximum side-on impulse (Fig 9). Additional data are included for the cylinder torso surrogates, exposed with the same setup. Scenarios at a HoB of 22 cm were reproduced with 0.2 kg and 0.4 kg of C-4.

For the range of maximum incident impulse covered, no significant differences and no tendencies can be noticed in terms of acceleration between the two reduced-scale surrogates. Nevertheless, discrepancies in their behaviours are observed with the other parameters (Vmax, Dmax and VCmax). Indeed, the maximum of velocity of the loaded surface is around two times higher for the RPP model than the cylinder one. For the maximum displacement and the VCmax, the response of the RPP is 3.5 times and 5 times higher than the cylinder one respectively. In those scenarios, the viscous criteria would predict a 5% risk of AIS>3 (thoracic injury) for the RPP, against less than 1% for the cylinder.

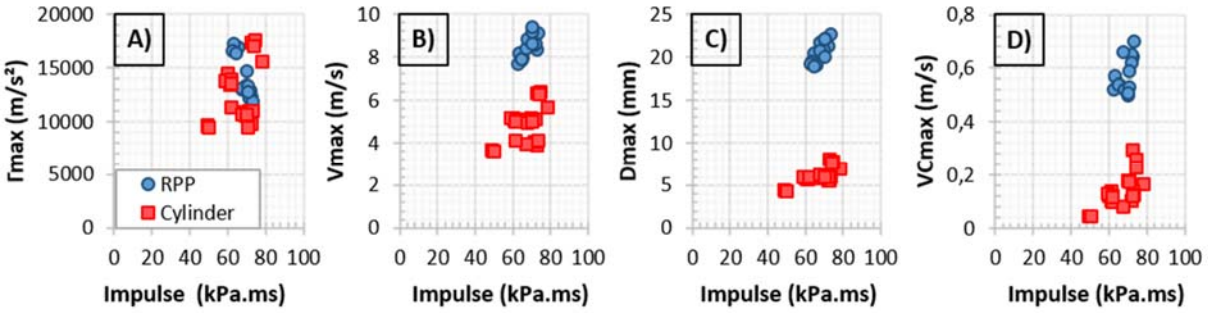

Fig. 9. Response of the RPP and the cylinder reduced-scale torso surrogates in terms of: (A) acceleration; (B) velocity; (C) displacement; and (D) VC. The maximum of those parameters are plotted against the maximum side-on impulse.

IV. DISCUSSION

The blast phenomenon is mainly characterised by its scale of very short duration, in which the simplest pressure profile is described with the Friedlander waveform. This profile gains in complexity as reflections are added (ground, wall, or obstacle). After the detonation of the explosive charge, the biological structures placed around can be damaged by the shockwave [1-2].

Although the soldiers are not only facing idealised shocks, most of the studies on blast interaction have used this pressure waveform [22-25]. It is therefore important to evaluate the influence of a complexification of the pressure wave on simplified torso surrogate's responses. The investigation of the pressure-time history influence on parameters such as received pressure and kinematic parameters was performed on simplified rigid and deformable torso-surrogates (RPP & Cylinder). Interaction of Friedlander wave on surrogates was performed, in addition to interaction with two separate shocks. Different pressure profiles were chosen because the detonation probably not always happened in free-field, means that the pressure profile will gains in complexity due to reflection on obstacles. For that reason, the influence of different pressure profile of similar impulse on the measured kinematic parameters was study.

Pressure around structures

The flow of a shock-wave around those structures was already well known [26-29], in addition to phenomena related to the interaction of the wave, such as diffraction and rarefaction waves. This phenomenon has previously been observed in experimental and numerical studies [25][29-31]. The time of arrival of the rarefaction wave and its amplitude depend not only on the distance between the measurement point and the edges but also on the incidence of the wave according to the loaded face [31]. The clearing effect has been known for decades, and it is possible to predict the influence of such phenomena on a plane surface loaded by a Friedlander wave impinging with a normal incidence [32-34].

In our cases, none of the scenario tested fills all those assumptions, preventing any comparison of our data with the existing model. Indeed, there is no prediction tool to evaluate the clearing effect for oblique blast wave interaction with structures, nor does one exist for normal wave interaction with non-planar structure, such as the cylinder in our study.

Changing the rigid material to a deformable one induces a reduction in the measured reflected impulse. This reduction is due to a transfer of a part of the impulse to the deformable membrane and is more important for the RPP. This is related, at least in part, to the fact that the displacement of the RPP is more than 3 times higher than the cylinder's one (20 mm against 6 mm).

Side-on pressure profile influence on kinematic parameters

It was shown that for different pressure profiles of similar maximum impulse, Γmax is different. Indeed, Γmax decrease when increasing the HoB. As those maxima are reached around 0.2 ms after the arrival of the side-on shock and as the ground reflection does not have reached the structure yet for the HoB 44 and 88 cm, this decrease was predictable. Indeed, only the first overpressure impinges the target at that time, this one being

higher in the Mach stem regime (HoB 22 cm). The reflected impulse is 1.5 to 2 times higher in the 22 cm HoB scenario when Γmax is attained. However, looking at this parameter against the maximum incident impulse show that no tendencies are observed, and that the shape does not have an influence on that parameter.

In contrast, for Vmax and Dmax, no tendencies are noticed according to the HoB. The 44 cm HoB scenario is either close to the HoB of 22 cm or the HoB of 88 cm, depending on the target's shape and the parameter considered, but fits can be obtained when plotting those parameters against the incident impulse, those fits being different according to the shape of the surrogates. It would then be interesting to know if those results are similar for another incident impulse.

With the aim to qualitatively or quantitatively evaluate the risk arising from the wearing of protective clothing on a dummy, it is necessary to have adapted criteria that are not influenced by the pressure profile, such as Vmax or Dmax, in addition to a reliable dummy. Although Vmax was shown not to be affected by the pressure waveform, it was shown that it is not a good metric to differentiate protective systems [8]. But this study [8] concluded that the peak of acceleration could be a good candidate parameter for this aim. Indeed, Γmax against the incident overpressure fits were found for the unprotected and protected MABIL surrogate, showing similar results than in the literature. However, those fits do not take into account the full pressure-time history and depending on this profile, different Γmax can be obtained for similar overpressure, as previously shown. In addition, for a quantitative assessment, those results suggest that the overpressure governs the injury for short-duration wave. Nevertheless, it is known for decades that it is in fact the incident impulse which is related to injuries and not the incident overpressure [35]. The current study shows that for similar impulse, different Γmax can be obtained that are not dependent on the surrogate shape. It means that no specific tendency can be obtained between Γmax and the maximum side-on impulse from any blast waves. This raises important issues to evaluate protective systems efficiency.

Additional tests on those simplified surrogates with others impulses could be useful to confirm those results. This could be performed experimentally or numerically. Indeed, the present reproducible data can be used to validate the numerical surrogate's models, which can then be used to performed additional scenarios. Moreover, future tests could be performed with an ellipsoidal shape which is more representative of the human torso shape. Though the reliability of the use of those manikins to reproduce human or mammal response remains unknown, experimental studies should be performed to measure the studied parameters on mammal in order to see if one of those dummy or torso surrogates can mimic its thoracic response. Moreover, injury from biological model exposed to such scenarios could also give important information.

V. CONCLUSIONS

In order to protect soldier and law enforcement officers from the increased IED threat, an important step is to understand the interaction of shock-wave with the concerned targets, and to know the pressure level and the motion for possible scenarios encountered in the battlefield.

Four reduced-scale simplified torso surrogates (two RPP and two cylinders) were exposed to several threats, corresponding to an explosive charge on the ground, to an explosive charge at the mid-thorax height of a man, and to an intermediate scenario.

From the rigid surrogates, it was shown that the impulse was indeed higher in the RPP faces which offer more surface to the blast than the cylindrical shape. Those impulses are then decrease in case of deformable structures. This decrease is related to the global motion of the membrane, which also depend from the shape of this one.

Those two deformable reduced-scale simplified torso surrogates were compared in terms of kinematic parameters. The RPP and the cylinder have similar trends in terms of maximum of acceleration for the range of impulse tested, but the behaviour of those models is different in terms of velocity and displacement. Next step would be to known if one of those simplified torso surrogates have similar behavior than the biological model.

Moreover, to qualitatively or quantitatively evaluate a protective system efficiency on a dummy, an adapted criterion is needed, which is unaffected by the pressure waveform. Even if a study from Ouellet [8] showed that Vmax is not adapted to differentiate protective system efficiency, this study showed that Vmax and Dmax could be good candidate parameters for thoracic injury criteria definition.

VI. ACKNOWLEDGEMENT

This work was partially supported by the French ANR program ASTRID (ANR- 12-ASTR-0025), led by the French Ministry of Defense, Direction Générale de l'Armement (DGA), under the contract "BLASTHOR".

VII. REFERENCES

[1] Mayorga, M.A. (1997) The Pathology of Primary Blast Overpressure Injury. *Toxicology*, **121**: pp.17–28.

[2] Phillips, Y.Y. (1986) Primary Blast Injuries. *Annals of Emergency Medicine*, **15**: pp.1446–50.

[3] Belmont, P.J., Schoenfeld, A.J., Goodman, G. (2010) Epidemiology of Combat Wounds in Operation Iraqi Freedom: Orthopaedic Burden of Disease. *Journal of Surgical Orthopaedic Advances*.

[4] icasualties.org. Afghanistan coalition casualty count. Available at: http://icasualties.org/OEF/index.aspx (accessed: 18 March 2015).

[5] Johnson, D.L., Yelverton, J.T., Hicks, W., Doyal, R. (1993) Blast Overpressure Studies with Animals and Man: Biological Response to Complex Blast Waves. *Final Report, US Army Medical Research and Development Command*.

[6] Teland, J.A. (2012) Review of Blast Injury Prediction Models. *FFI-rapport 2012/00539*.

[7] Magnan, P., De Mezzo, S., Heck, S., Boehrer, Y. (2011) Approche métrologique du chargement d'une membrane exposée au blast. Rapport S-R 123/2011 de l'Institut Franco-Allemand de Recherches de Saint-Louis, France.

[8] Ouellet, S., Williams, K. Characterisation of Defence Research and Development Canada's Mannequin for the Assessment of Blast Incapacitation and Lethality (DRDC MABIL). *Proceeding of PASS* conference, 2008, Brussels.

[9] Axelsson, H., Yelverton, J.T. (1996) Chest Wall Velocity as a Predictor of Nonauditory Blast Injury in a Complex Wave Environment. *The Journal of Trauma*, **40**(3).

[10] Stuhmiller, J.H., Ho, K.H.H., *et al.* (1996) Model of Blast Overpressure Injury to the Lung. *Journal of Biomechanics*, **29**(2): pp.227–34.

[11] Teland, J.A., Van Doormaal, J.C.A.M., Van der Horst, M.J., Svinsas, E. (2010) A single point pressure approach as input for injury models with respect to complex blast loading conditions. *Proceeding of the MABS 21st*, Jerusalem, Israel.

[12] Van der Voort, M.M., Holm, K.B., *et al.* (2016) A new standard for predicting lung injury inflicted by Friedlander blast waves. *Journal of Loss Prevention in the Process Industries*, **40:** pp.396-405.

[13] Bowen, I.G., Fletcher, E.R., Richmond, D.R. (1968) Estimate of Man's Tolerance to the Direct Effects of Air Blast. *Technical progress report no. DASA-2113, Department of Defense, Defense Atomic Support Agency*, Washington, D.C.

[14] Bass, C.R., Rafaels, K.A., Salzar, R.S. (2008) Pulmonary Injury Risk Assessment for Short-Duration Blasts. *The Journal of Trauma*, **65**: pp.60–615.

[15] Magnan, P., De Mezzo, S., Heck, S., Boehrer, Y. (2012) Approche métrologique du chargement par le blast de cibles anthropomorphiques instrumentées - Essais ISL/DGA Tt. Rapport S-R 108/2012 de l'Institut Franco-Allemand de Recherches de Saint-Louis, France.

[16] Bouamoul, A., Williams, K., Lévesque, H. Experimental and Numerical Modelling of a Mannequin for the Assessment of Blast Incapacitation and Lethality under Blast Loading. *Proceeding of the 23rd International Symposium on Ballistics*, 16–20 April 2007, Tarragona (Spain).

[17] Boutillier, J., Deck, C., Magnan, P., Naz, P., Willinger, R. (2016, in press) A critical review on primary blast thorax injury and their outcomes. *Journal of trauma*. DOI: 10.1097/TA.0000000000001076

[18] Ehrhardt, L., Boutillier, J., *et al.* (2016) Evaluation of overpressure prediction models for air blast above the triple point. *Journal of Hazardous Materials*, **311**: pp.176-185.

[19] Ehrhardt L, Boutillier J, Magnan P, Deck C, De Mezzo S, Willinger R. Blast with ground reflection, a real scaled experimental and numerical study. *Proceeding of MABS 23rd conference*, 2014, Oxford.

[20] Smooth-on, Liquid Rubbers and Plastic for Artists and Industry, http://www.smooth-on.com/tb/files/PMC_770_TB.pdf (accessed : March 2016).

[21] Lau, I.V., Viano, D.C. The Viscous Criterion – bases and applications of an injury severity index for soft tissues. *Proceeding of the Thirtieth Stapp Car Crash Conference*, 1986, SAE Paper No. 861882, pp. 123-142.

[22]Richmond, D.R., Damon, E.G., Bowen, I.G., Fletcher, E.R., White, C.S. (1966) Air-Blast Studies with Eight Species of Mammals. Technical Progress Report, DASA-1854, Defense Atomic Support Agency, Department of Defense, Washington D.C.

[23]Dodd, K.T., *et al.* (1991) The effects of Pulmonary Contusion on Cardiopulmonary function in Sheep. Federation Proceeding.

[24]Vassout, P., *et al.* (1996) Comparaison des lésions extra-auditives chez le mouton exposé à une onde de choc en champ libre et au moyen d'un tube à choc de faible diamètre. Rapport R 117/96 de l'Institut Franco-Allemand de Recherches de Saint-Louis, France.

[25]Tyas, A., Warren, J.A., Bennett, T., Fay, S.D. (2011) Prediction of clearing effects in far-field blast loading of finite targets. *Shock Waves*, **21**(2): pp.111–119.

[26]Hillier, R. Numerical modelling of shock wave diffraction. *Proceeding of 19th international symposium on shock waves*, Marseille IV: pp.117-122.

[27]Drikakis, D., Ofengeim, D. (1997) Computation of non-stationary shock-wave/cylinder interaction using adaptive-grid methods. *Journal of Fluids and Structures,* **11**: pp.665-691.

[28]Brown, C.J., Thomas, G.O. (2000) Experimental studies of ignition and transition to detonation induced by the reflection and diffraction of shock waves. *Shock Waves*, **10**: pp.23-32.

[29]Rigby, S.E., Tyas, A., Bennett, R., Warren, J.A., Fay, S.D. (2013) Clearing effects on plates subjected to blast loads. *Engineering and Computational Mechanics*, **166**(3): pp.140–148

[30]Shi, Y., Hao, H., Zhong-Xian, L. (2007) Numerical simulation of blast wave interaction with structure columns. *Shock Waves*, **17**: pp.113–133.

[31]Rose, T.A., Smith, P.D., May, J.H. (2006) The interaction of oblique blast waves with buildings. *Shock Waves*, **16**: pp.35–44.

[32]Rigby, S.E., Tyas, A., Bennett, T., Fay, S.D., Clarke, S.D., Warren, J.A. (2014) A numerical investigation of blast loading on small targets. *International Journal of Protective Structures*, **5**(3): pp.253-274.

[33]US Department of Defense. Structures to resist the effects of accidental explosions. US DoD, Washington DC, USA, UFC-3-340-02, 2008

[34]Hudson, C.C. (1955) Sound pulse approximations to blast loading (with comments on transient drag). SC-TM-191-55-51, Sandia Corporation, MD, USA.

[35]Schardin, H. (1950) The Physical Principles of the Effects of a Detonation. Chap. 14-A, *German Aviation Medicine*, World War II, **2**: pp.1207–24.